Journal of Solid State Chemistry 327 (2023) 124251

Contents lists available at ScienceDirect

Journal of Solid State Chemistry

journal homepage: www.elsevier.com/locate/jssc

Nucleation & growth of α-$Ti(HPO_4)_2{\cdot}H_2O$ single-crystal and its structure determination from X-ray single–crystal data

Zakariae Amghouz [a,**], Rafael Mendoza-Meroño [b], Alaa Adawy [c,*]

[a] Department of Material Science and Metallurgical Engineering, University of Oviedo, 33203, Gijón, Spain
[b] Department of Physical and Analytical Chemistry, University of Oviedo, 33006, Oviedo, Spain
[c] Unit of Electron Microscopy and Nanotechnology, Institute for Scientific and Technological Resources (SCTs), University of Oviedo, 33006, Oviedo, Spain

ARTICLE INFO

Keywords:
Titanium phosphate
Nanolayered nanomaterials
Hydrothermal crystal growth
Single crystal growth
Single crystal X-ray diffraction

ABSTRACT

α-titanium phosphate phase [α-$Ti(HPO_4)_2{\cdot}H_2O$; abbreviated as α-TiP] is a nanolayered metal phosphate with several industrial and recent biotechnological applications related to their nanolayered morphology and ion exchange capabilities. Structural wise, α-TiP is a tetravalent metal phosphate that tends to crystallize into microcrystalline powder. Here we report that the crystallization of single α-TiP crystals with suitable dimensions (>50 μm) for single-crystal X-ray diffraction could be effectuated using a prolonged hydrothermal treatment of a metallic titanium alloy (Ti–6Al–4V) in a highly concentrated phosphoric acid aqueous solution. Accordingly, the single-crystal X-ray diffraction analysis revealed the crystalline structure in a monoclinic space group, $P2_1/c$, with a = 8.6288(5) Å, b = 5.00546(17) Å, c = 19.1468(11) Å, and β = 127.555(9)°. Although the space group is the same crystallographic space group that was previously reported from the microcrystalline powder relying on powder X-ray diffraction (PXRD) and neutron powder diffraction, the obtained unit cell volume is slightly larger. Bulk of the obtained crystals were also subjected to detailed analyses using polarization optical microscopy (POM), scanning electron microscopy combined with energy dispersive X-ray microanalysis (SEM-EDX), Fourier transform Infrared Spectroscopy (FTIR) and thermal analysis (TG/SDTA). The single crystals are hexagonally shaped and exhibit the exact titanium to phosphorus ratio expected for α-TiP. The bulk sample PXRD pattern resembles perfectly that reported for the α-TiP polycrystalline powder with clearly sharper peaks. TGA-SDTA analysis revealed the expected thermal behaviour for α-TiP phase and demonstrated their higher thermal stability when compared to the polycrystalline powder.

1. Introduction

α-titanium phosphate, with the chemical formula α-$Ti(HPO_4)_2{\cdot}H_2O$, (abbreviated hereafter as α-TiP), is a tetravalent metal phosphate, on which investigations started in the middle of 1960s in an attempt to reproduce the synthesis and applications of its preceding zirconium analogue (α-ZrP) [1–4]. Like α-ZrP, α-TiP has high capacity for ion exchange and could be functionalized and exfoliated through intercalation with amines and other ions (species) or could be used as a repository for bio-functional nanoparticles [5–16]. With the same nanolayered morphology, there exist two other compounds with the chemical formula γ-TiP [$Ti(PO_4)(H_2PO_4){\bullet}2H_2O$] and its anhydrous form β-TiP [$Ti(PO_4)(H_2PO_4)$] [17–22]. To our knowledge, none of these nanolayered structures nor the other nanofibrous titanium phosphates (**ρ**-TiP and its polymorph π-TiP) could be crystallized into single crystals suitable for single-crystal X-ray structural studies. This is because they all tend to crystallize in the form of polycrystalline powder and, therefore, this made it only possible to study the crystalline structure of these phases using neutron and X-ray (also lately synchrotron) powder diffraction and solid-state NMR [23–29]. These results allowed for obtaining valuable general information about the bulk crystallinity and an approximate depiction of their three-dimensional structures. Nevertheless, the possibility of solving structures using single-crystal XRD would undoubtedly allow for the observation of the absolute atomic positions, bond lengths and angles and thus the determination of their definite *pseudo* 3D crystalline structure. For this the nucleation and crystal growth of high-quality crystals suitable for single crystal studies are the limiting factors [30–33]. Several methods have been reported to

* Corresponding author.
** Corresponding author.
E-mail addresses: amghouzzakariae@uniovi.es (Z. Amghouz), hassanalaa@uniovi.es (A. Adawy).

https://doi.org/10.1016/j.jssc.2023.124251
Received 4 April 2023; Received in revised form 30 July 2023; Accepted 2 August 2023
Available online 8 August 2023

effectuate the growth of high-quality crystals for inorganic, organic, or hybrid (macro-) molecules at different size scales [34–38]. However, obtaining single crystals in the case of a metal phosphate such as **α**-TiP is a three-step process, the first of which is the chemical reaction that would mediate the production of the required chemical compound [39]. Many studies reported on the synthesis of **α**-TiP, the first step of which is the synthesis of an amorphous titanium phosphate that is then treated hydrothermally with phosphoric acid solutions to be converted to a polycrystalline phase and this is indeed the reason for the difficulty of obtaining high-quality single crystals of appropriate sizes for single crystal XRD studies, because the immediate high supersaturation that results of that mixture would indeed decrease any possibility for single crystal growth [40,41]. Therefore, changing the starting materials source and/or decreasing the supersaturation could facilitate the route to more controlled nucleation and crystal growth.

Here we report our approach to effectuate the growth of α-TiP single crystals using a 3-day hydrothermal treatment of a titanium alloy (Ti–6Al–4V) that is regularly used for medical applications [42,43]. This hydrothermal treatment in phosphoric acid aqueous solution allowed for the controlled formation of α-TiP growth units through the slow formation of titanium cations (Ti^{4+}), due to the slow corrosion of the titanium alloy (substrate), and their subsequent reaction with hydrolysed phosphate groups (HPO_4^{2-}). Afterwards, the α-TiP growth units heterogeneously nucleated on the titanium alloy surface and continued their growth as 3D crystals through the 2D nucleation mechanism, as was revealed using the microscopic inspection. The crystals grew to dimensions that allowed for an unprecedented determination of the crystalline structure from single-crystal XRD data, that largely coincided with the crystal structure obtained previously for the polycrystalline powder using neutron powder diffraction [44,45]. The obtained crystals were also studied using POM, FTIR, SEM-EDX, PXRD and TGA and the results confirmed that the resultant crystals bear almost the same structural properties of the polycrystalline powder with a higher thermal stability.

2. Materials and methods

2.1. Crystallization of α-TiP single-crystals

Ti–6Al–4V discs of 1 mm thickness and 5 mm diameter (*c.a.* 0.55 g of titanium) were cut and cleaned thoroughly using sonication in acetone, ethanol and distilled water, each for 10 min, respectively, and picked out to dry on dust-free papers. In a typical experiment, a disc was immersed in a 5 mL of 5 M H_3PO_4 aqueous solutions and hydrothermally treated at 180 °C for 3 days under autogenous pressure using well-sealed Teflon-lined stainless-steel autoclaves of 40 mL volume capacity. Afterwards, the autoclaves were left to cool down to room temperature. The grown single crystals were filtered, washed thoroughly with distilled water, and finally air-dried in an oven at 40 °C.

2.2. Structural characterization methodologies

2.2.1. Single-crystal X-ray diffraction studies

Data collection was performed on an Oxford Diffraction Gemini S single-crystal diffractometer, using monochromatic radiation. Images were collected at a 55 mm fixed crystal–detector distance, using the oscillation method, with variable exposure time per image. The sample was measured using CuKα radiation (λ = 1.5418 Å) at 120 K. The crystal structure was solved by direct methods and refined by full-matrix least squares on F^2. The complete model, except H atoms, was indicated by the direct-methods program *SIR*2014 [46]. The atomic positions were introduced in the program *Olex2* [47] and refined from a least-squares calculation. The H atoms were added geometrically to the model.

2.2.2. Morphological characterization

Polarization optical microscopy (POM) images were obtained using an automated optical microscope Olympus BX61 for transmission and fluorescence studies equipped with a motorized stage and a high-resolution digital camera Olympus DP-70 (12Mega pxiels).

Scanning electron microscopy (SEM) micrographs and energy dispersive X-ray microanalysis (EDX) were recorded with a JEOL JSM-6100 scanning electron microscope (JEOL, Tokyo, Japan) operated at 20 kV coupled with an energy dispersive X-ray microanalysis (EDX) with an X-Max silicon drift (SDD) 80 mm^2 detector (Oxford instruments, High Wycombe, England).

2.2.3. Phase characterization

The Fourier transform Infrared Spectroscopy (FTIR) for the polycrystalline and single crystal α-TiP were recorded in the range of 4000–600 cm^{-1} with an FTIR spectrophotometer, attached to a microscope with an image-forming system (Varian 620-IR and Varian 670-IR) and three detection systems: one located in the spectrometer and two in the microscope (FPA, for imaging and MCT). Samples were used as-is, thanks to the used mode of the attenuated total reflectance.

2.2.4. Powder X-ray diffraction studies

The powder X-ray diffraction (PXRD) pattern was recorded on an X'Pert diffractometer (Philips, Amelo, The Netherlands) with Cu-Kα radiation (λ = 1.5406 Å) at room temperature over the angular 2θ range 5–90° with a step of 0.02° and a counting time of 1.5 s/step. Rietveld refinement was carried out by the FullProf program [48]. Our single crystal structure of α-TiP was used as the initial model. The PXRD profile has been modeled as a Pseudo-Voigt function in the range 2θ = 5–90°. The zero offset, the scale factor, background (Linear Interpolation between a set background points with refinable heights), the unit cell, fwhm and shape parameters, asymmetry correction for peaks below 2θ = 20°, and the atomic positions and anisotropic temperature factors of Ti, P, and O atoms (excepting H) were refined.

2.2.5. Thermal characterization

A Mettler-Toledo TGA/SDTA851^e was used for the thermal analyses in oxygen and nitrogen dynamic atmospheres (50 mL/min) at a heating rate of 10 °C/min. In all cases, ca. 20 mg of powdered sample was thermally treated, and blank runs were performed.

3. Results and discussion

Using the hydrothermal treatment of Ti–6Al–4V alloy in aqueous phosphoric acid solution, that resulted in a reaction crystallization mechanism, led to the growth of platy hexagonally shaped α-TiP crystals reaching an average size of 50–100 μm in their largest dimension and 10 folds lower values (<10 μm) in their smallest dimension, i.e., the crystal thickness, as revealed through the optical microscopy observations (Fig. 1). This indicates that, unlike the usually obtained sub-microcrystalline powder for α-TiP (around 100 nm) through conventional synthesis approaches [7,10–14,16], using this hydrothermal crystallization methodology allowed for: 1) controlled corrosion of the titanium disc, that in turn led to; 2) controlled dissolution of the titanium ions into the phosphoric acid aqueous solution, that 3) under the hydrothermal conditions had undergone decomposition to different phosphate groups. The controlled titanium ions release into the system is indeed the way we controlled the supersaturation levels to be the lowest possible and therefore this minimized the nucleation events and allowed crystals to grow to relatively larger sizes. This is unlike the other methods where all the free titanium ions are put in direct vicinity reactive conditions with the phosphorous ions, leading to immediate high supersaturation levels and thus uncontrolled nucleation and polycrystallinity. Worth mentioning is that the hydrothermal treatment was performed in a relatively narrow cylindrical autoclave (surface area = 7 cm^2) and thus due to gravitational forces, the formed solid phases would settle at the bottom, possibly on the disc surface, before the complete dissolution of the whole disc, leaving behind isolated crystals. An overall

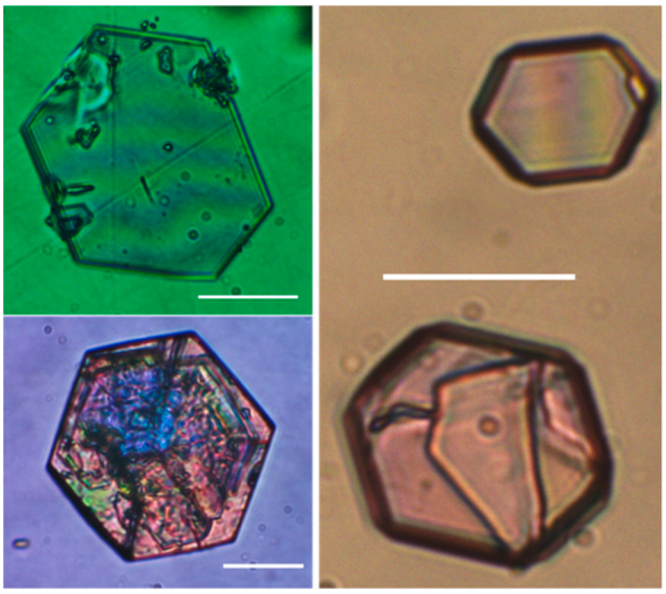

Fig. 1. Polarization optical microscopy images for single-crystals of α-Ti $(HPO_4)_2{\cdot}H_20$. Scale bar: 50 μm.

look to the obtained crystals, shows that around 25% of the obtained crystals have successfully grown to crystals of good quality. Particularly, smaller-sized crystals have better crystal surfaces when compared to the larger crystals that mostly have their surfaces blocked with irregularities and defects, possibly through secondary heterogeneous nucleation on their surfaces (Fig. 1).

Scanning electron microscopy confirmed the size aspects and revealed that the crystals grew in a layered pattern with 2D nucleation as the main regime of crystal growth, while screw dislocations wherever detected led to spiral growth of polycrystals or the growth of relatively much larger crystals with weak or no diffraction ability (Fig. 2).

Energy dispersive X-ray microanalysis (EDX) was performed on several crystals, and the normalized titanium to phosphorus atomic percentage ratio (Ti:P %atom) for all examined crystals was 1:2, which is the theoretically expected value for this compound [α-$Ti(HPO_4)_2{\cdot}H_2O$] (Fig. 3).

As another important aspect, the synthesis was carefully evaluated after different periods of hydrothermal incubation to reveal the nucleation mechanism. SEM inspection of the Ti–6Al–4V discs incubated for 3 and 4 h in this reactive crystallization conditions showed that the disc started to experience its surface corrosion with almost no detected phosphorous and Ti to Al to V proportions very close to the theoretical values of that alloy (Fig. S1). However, in the solution, this etching led to increasing the amount of titanium ions (most probably Ti^{4+}, since TiO_2 forms easily upon subjecting titanium to oxygen containing medium) in the solution, leading to the formation of the very first titanium phosphate phases (Fig. S2). It is important to mention here that although the disc etching should have released Al^{3+} and V^{5+} cations, they were almost not detectable in the areas where crystalline nuclei sediments were detected on the disc surface (Fig. S2). SEM imaging of the Ti–6Al–4V discs after 6 h in the same conditions showed tiny crystals covering the disc surface, indicating possible heterogenous nucleation, before they continued their crystal growth to completely exhaust (dissolve) the discs (the titanium source) (Fig. 4). At this early stage, Ti:P %atom obtained with EDX analysis showed various values (Fig. S3). This could be attributed to the presence of different phosphate groups form in the reactive solution ($H_2PO_4^-$, HPO_4^{2-} and/or PO_4^{3-}), and thus the formation of different TiP phases at the early stage of the hydrothermal treatment [49–51].

The spectroscopic characterization of the vibration modes of the polycrystalline powder and single crystals of α-TiP coincided perfectly,

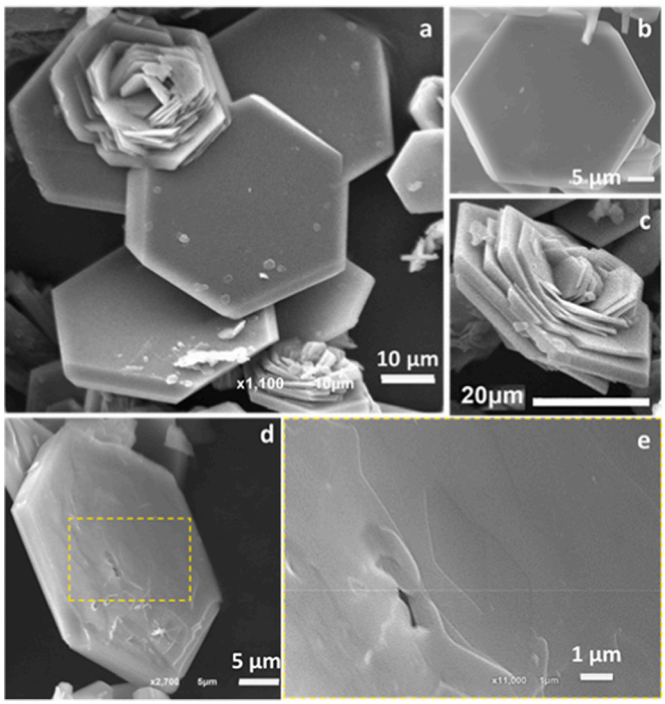

Fig. 2. Scanning electron microscopy images for crystals of α-$Ti(HPO_4)_2{\cdot}H_20$. The images confirm the crystal habit, size, and final morphology (a). Crystals of relatively smaller sizes show smooth surfaces (b). Stacked crystals appear to be a result of spiral crystal growth relying on screw dislocations (c). At high magnification, islands of 2D nucleation were observed on the surface of relatively smooth-surfaced crystals (d,e).

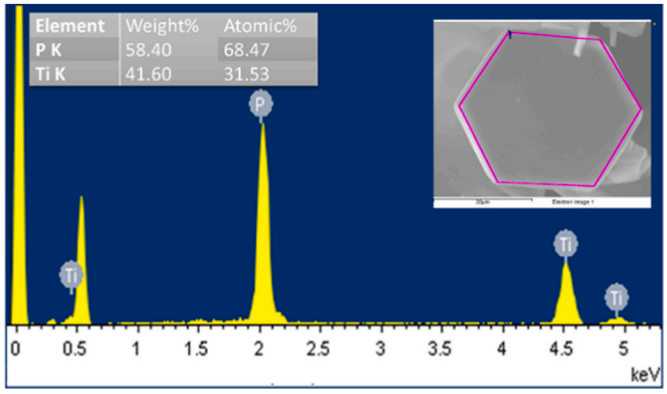

Fig. 3. Representative EDX for a single α-$Ti(HPO_4)_2{\cdot}H_20$ crystal showing the normalized atomic and weight percentage ratio of titanium to phosphorus that coincides with its exact chemical formula.

but the single crystals showed relatively lower transmittance and thus higher absorbance at most of the vibration bands compared to those resulting from the polycrystalline powder (Fig. 5). This implies that there is a higher population of bonds which have vibrational energies corresponding to the incident light in the single crystals when compared to the polycrystalline powder. The bands corresponding to the OH functional groups of water, the OH of the P–OH group, the P–O and P═O of PO_4^{3-} and PO_3^{2-} of HPO_4^{2-}, and the terminal group Ti–O were detected. The bands at 3550 cm^{-1} and 3475 cm^{-1} are attributed to stretching vibrations of the OH groups in the molecular water that was adsorbed and crystallized in the region of the inter-laminar structure. The absence of a band at 3249 cm^{-1} (that only is shown as a hardly defined shoulder) indicates that our material is dehydrated. The wide band around 3000 cm^{-1} indicates a strong union between the phosphate groups and the

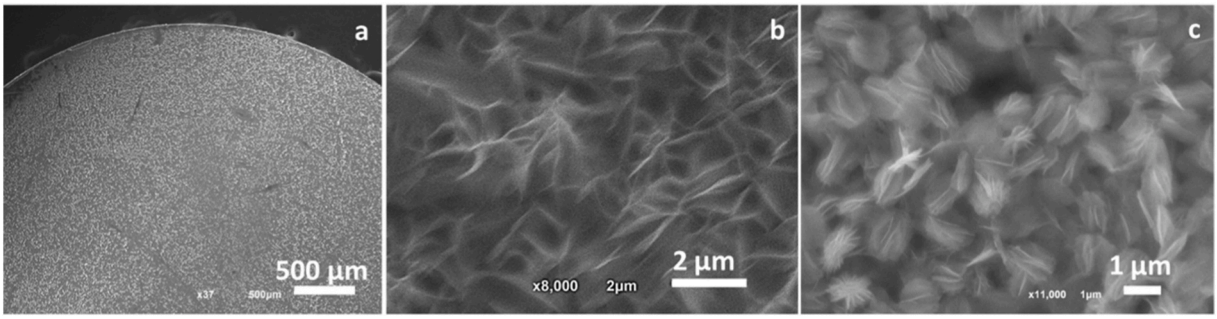

Fig. 4. SEM microscopy for the Ti–6Al–4V discs after their hydrothermal treatment in phosphoric acid aqueous solutions for 6 h at low (a) and high magnifications (b) and after 12 h (c), showing the early heterogenous nucleation of the α-Ti$(HPO_4)_2{\cdot}H_20$ crystals on the disc surface.

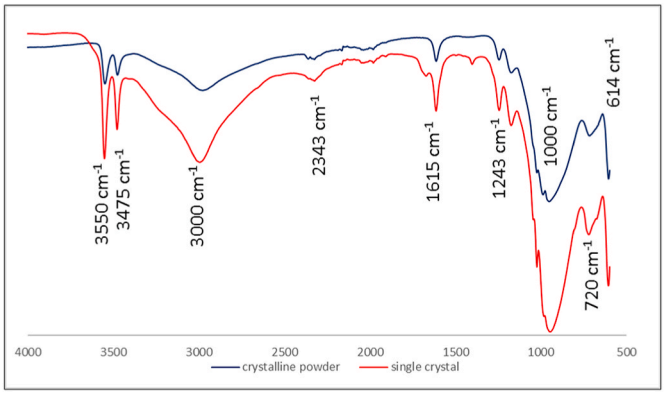

Fig. 5. FTIR spectra of the synthesized polycrystalline powder (blue) and single crystals (red) of α-TiP obtained by scanning from 4000 to 600 cm^{-1}.

titanium atoms in the Ti–O–P angle. Bands around 1615 cm^{-1} are attributed to the H–O–H angle that generates a bending vibration of the water molecules coordinated with phosphate groups. A shoulder is observed at 1243 cm^{-1} accounts for the asymmetrical stretching vibration mode of P–OH. The presence of multiple bands around that wavenumber range can also imply the effect of the stretching mode of the P═O bond. Around 1000 cm^{-1}, big band with multiple minima occurs that can be attributed to vibration modes for the symmetrical and asymmetrical stretching of P–O, out-of-phase with the PO_4^{3-} and HPO_4^{2-}. Finally, the bands appearing around 720 and 614 cm^{-1} can be attributed to the P–OH group and the overlap of the Ti–O group [52–57].

Regarding the crystallographic aspects, the structure of α-Ti$(HPO_4)_2{\cdot}H_2O$ (α-TiP) was previously determined using neutron powder diffraction in combination with Rietveld refinement and Fourier synthesis [44]. The calculated $P2_1/c$ space group using single-crystal refinement is the same space group obtained using powder diffraction, but the unit cell parameters and thus the unit cell volume (Table 1) are around 0.6% larger than the previously obtained unit cell [$a = 8.6110(3)$ Å, $b = 4.9933(2)$ Å, $c = 16.1507(7)$ Å and $\beta = 110.206(3)^\circ$, Volume $= 651.70(5)$ $Å^3$]. This could be attributed to two factors, the first of which is the possible incorporation of impurities, especially that the substrate contains other elements than titanium [58,59]. Another possibility could be the non-avoided radiation damage that those platy crystals could have encountered due to the prolonged exposure to the X-ray beam [60]. The crystallographic data and details of the final least-squares refinement are summarized in Table 2. Bond lengths and angles are listed in Tables 3 and 4.

Powder X-ray diffraction analysis (PXRD) of the obtained bulk α-TiP crystals showed high crystallinity with much sharper peaks compared to that of the polycrystalline fine powder pattern, with the first characteristic peak at $2\theta = 11.651^\circ$ ($d_{002} = 7.5895$ Å), that corresponds to its interlayer spacing's. In order to verify the agreement of these new cell

Table 1
Crystal data and structure refinement for α-Ti$(HPO_4)_2{\cdot}H_20$ (a: single-crystal, b: powder [44]).

Empirical formula	$H_4O_9P_2Ti$ (a)	$H_4O_9P_2Ti$ (b)
Formula weight	257.87	257.87
Temperature/K	120	RT
Crystal system	Monoclinic	Monoclinic
Space group	$P2_1/c$	P21/c
a/Å	8.6288(5)	8.6110(3)
b/Å	5.00546(17)	4.9933(2)
c/Å	19.1468(11)	16.1507 (7)
β/°	127.555(9)	110.206(3)
Volume/$Å^3$	655.60(8)	651.70(5)
Z	4	4
$\rho_{calc}g/cm^3$	2.613	
μ/mm^1	16.107	No. of parameters: 71
F(000)	512.0	R_{wp}: 1.67
Radiation	Cu Kα (λ = 1.54184)	R_{exp}: 1.05
2Θ range for data collection/°	10.926 to 151.3	R_F: 4.45
Index ranges	$-7 \le h \le 10, -6 \le k \le 4, -23 \le l \le 21$	χ^2: 2.54
Reflections collected	3926	
Independent reflections	1330 [$R_{int} = 0.0625$, $R_{sigma} = 0.0710$]	
Data/restraints/parameters	1330/0/114	
Goodness-of-fit on F^2	1.053	
Final R indexes [$I \ge 2\sigma(I)$]	$R_1 = 0.0450$, $wR_2 = 0.1008$	
Final R indexes [all data]	$R_1 = 0.0725$, $wR_2 = 0.1182$	
Largest diff. peak/hole/e $Å^{-3}$	0.52/-0.56	
CCDC no.	2124760	

Table 2
Bond Lengths for α-Ti$(HPO_4)_2{\cdot}H_20$.

Atom	Atom	Length/Å	Atom	Atom	Length/Å
Ti1	O3[a]	1.954(4)	P1	O6	1.506(4)
Ti1	O4	1.932(4)	P1	O7	1.516(4)
Ti1	O6	1.948(4)	P1	O9[c]	1.522(4)
Ti1	O7[b]	1.907(4)	P2	O1	1.552(4)
Ti1	O8	1.914(4)	P2	O3	1.520(4)
Ti1	O9	1.940(4)	P2	O4	1.527(4)
P1	O5	1.569(4)	P2	O8[d]	1.523(4)

Symmetry code.
[a] -X,1-Y,2-Z.
[b] 1-X,-Y,2-Z.
[c] +X,-1+Y,+Z.
[d] +X,1+Y,+Z.

Table 3
Bond Angles for α-Ti$(HPO_4)_2{\cdot}H_2O$.

Atom	Atom	Atom	Angle/°	Atom	Atom	Atom	Angle/°
O4	Ti1	O3[a]	89.23(17)	O6	P1	O9[3]	111.1(2)
O4	Ti1	O6	178.84(17)	O7	P1	O5	108.8(2)
O4	Ti1	O9	91.88(16)	O7	P1	O9[3]	110.7(2)
O6	Ti1	O3[a]	89.63(17)	O9[c]	P1	O5	109.7(2)
O7[2]	Ti1	O3[a]	178.66(18)	O3	P2	O1	104.3(2)
O7[2]	Ti1	O4	89.47(17)	O3	P2	O4	111.0(2)
O7[2]	Ti1	O6	91.67(17)	O3	P2	O8[d]	112.4(2)
O7[2]	Ti1	O8	89.92(17)	O4	P2	O1	109.2(2)
O7[2]	Ti1	O9	90.22(17)	O8[d]	P2	O1	108.6(2)
O8	Ti1	O3[a]	90.43(17)	O8[d]	P2	O4	111.0(2)
O8	Ti1	O4	90.80(17)	P2	O3	Ti1[a]	141.1(3)
O8	Ti1	O6	89.01(16)	P2	O4	Ti1	142.4(2)
O8	Ti1	O9	177.32(17)	P1	O6	Ti1	141.8(2)
O9	Ti1	O3[a]	89.48(16)	P1	O7	Ti1[b]	152.0(3)
O9	Ti1	O6	88.31(16)	P2[3]	O8	Ti1	149.0(2)
O6	P1	O5	103.4(2)	P1[4]	O9	Ti1	141.3(2)
O6	P1	O7	112.8(2)				

Symmetry code.
[a] -X,1-Y,2-Z.
[b] 1-X,-Y,2-Z.
[c] +X,-1+Y,+Z.
[d] +X,1+Y,+Z.

Table 4
Geometry of Hydrogen bond (Å, °) for α-Ti$(HPO_4)_2{\cdot}H_2O$.

Donor –H···Acceptor	D-H	H···A	D···A	D - H···A
O1–H1···O2	0.82	1.92	2.723(8)	166
O2–H2a···O3	0.71	2.38	3.047(6)	157
O2–H2b···O5	0.86	2.14	2.984(7)	166
O5–H5···O2	0.82	192	2.737(7)	175

parameters with the experimental PXRD pattern of the bulk sample of α-TiP, Pawley fitting method was performed with our generated CIF file and the experimental powder pattern (blue pattern) using the program High Score Plus [61]. The R_{wp} (= 8.15) and goodness-of-fit (χ^2 = 1.64) values show a good agreement, which means that the obtained unit cell found by single-crystal XRD study reproduces the experimental PXRD diagram and these values are reliable (Fig. 6). Moreover, the final Rietveld refinement plot is given in Fig. 7, while crystallographic and refinement data are reported in Table S1. The obtained crystallographic and refinement data confirms the proposed unit cell found by single-crystal XRD study for α-TiP.

The asymmetric unit cell of α-TiP comprises one Ti^{4+} cation, two HPO_4^{2-} anions, and one water molecule (Fig. 8a). In α-TiP, Ti^{4+} cation occupies a slightly distorted octahedral environment (Fig. 8b), being surrounded by six Ti–O bonds belonging to two crystallographically non-equivalent PO_4 tetrahedra of HPO_4^{2-} anions (Fig. 8c and d). Out of the six oxygen atoms coordinated to Ti^{4+} cation, each three come from three crystallographically equivalents PO_4 tetrahedra of HPO_4^{2-} anions (Fig. 8e). The Ti–O interatomic distances range from 1.907(4) to 1.954 (4) Å, with the average values of 1.933(4) Å, are reasonable and comparable to those found in the α-TiP previously determined using neutron powder diffraction in combination with Rietveld refinement and Fourier synthesis [44]. Moreover, the bond lengths and angles are in agreement with those value found for analogous Ti^{4+} octahedral geometries from CDS (Cambridge Data Base-2020) [62]. The two mono-hydrogen phosphate groups, HPO_4^{2-}, crystallographically non-equivalent with tetrahedral geometry are vertex-shared with $\{TiO_6\}$ octahedra, and each PO_4 tetrahedron shares three of its four oxygen atoms with Ti^{4+} cation, while the fourth is linked to a hydrogen atom, constituting the most active site in α-TiP material (Fig. 8f and g). The P–O bonds range from 1.506(4) to 1.569(4) Å, with the average values of 1.529(4) Å. These vertex-shared PO_4 tetrahedra with $\{TiO_6\}$ octahedra gives rise to 2D-inorganic sheets in the *ab*-plane with an interlayer spacing of 7.59 Å (See the first diffraction peak in PXRD pattern in Fig. 6). In these inorganic sheets, the monohydrogen phosphate groups are located alternatively up and down each *ab*-plane containing the $\{TiO_6\}$ octahedra (Figs. 9 and 10). The packing of these inorganic layers generates six-sided cavities that contain the non-coordinated water molecules, which interact strongly

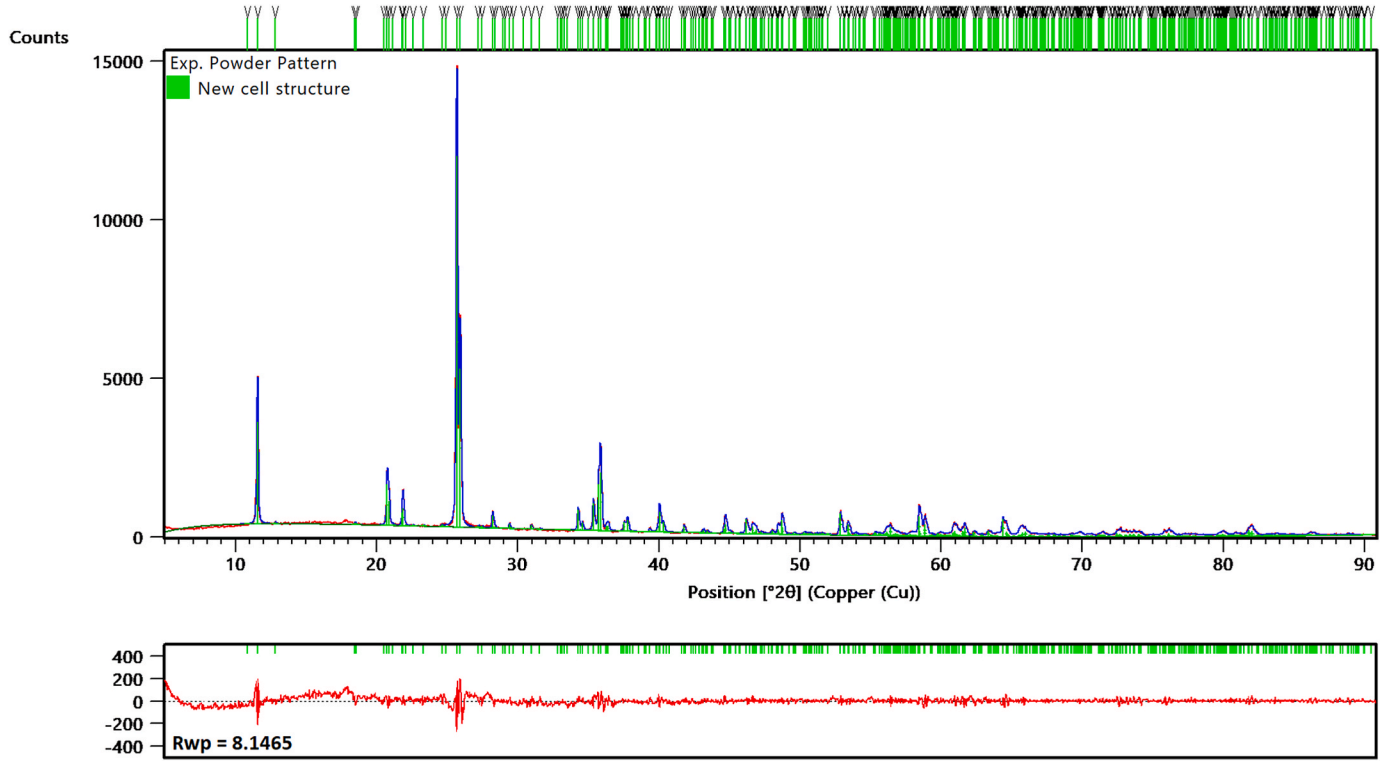

Fig. 6. Pawley fitting (green) of the experimental powder XRD pattern (blue) with the new obtained cell parameters and the difference curve for the fit (red).

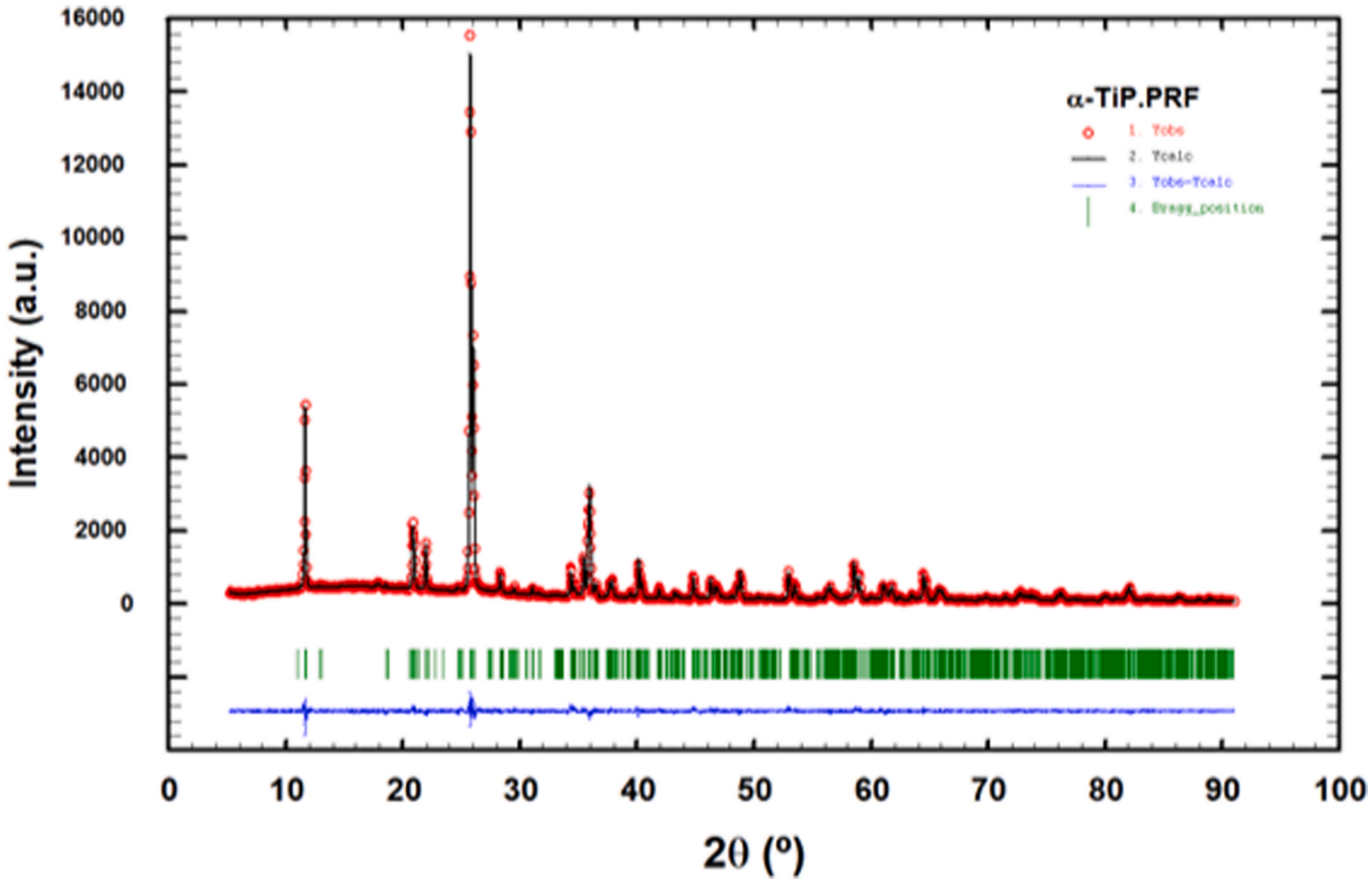

Fig. 7. Final Rietveld refinement plots showing the experimental (red circles), calculated (black line) and difference profiles (blue line); green tick marks indicate reflection positions.

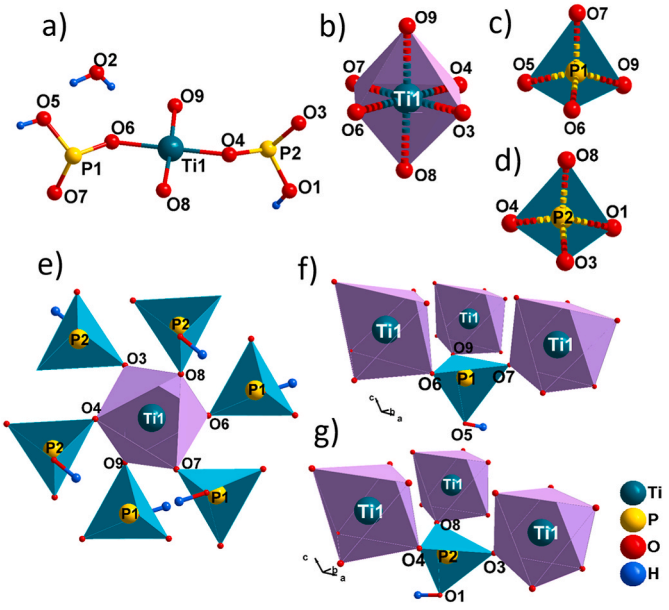

Fig. 8. Crystal structure details of α-Ti$(HPO_4)_2{\cdot}H_20$: asymmetric unit (a), perspective view of the coordination environment of Ti (b) and HPO_4^{2-} (c,d). Perspective view of the vertex-shared {TiO6}, {P(1)O_4} and {P(2)O_4} polyhedra (e,f,g).

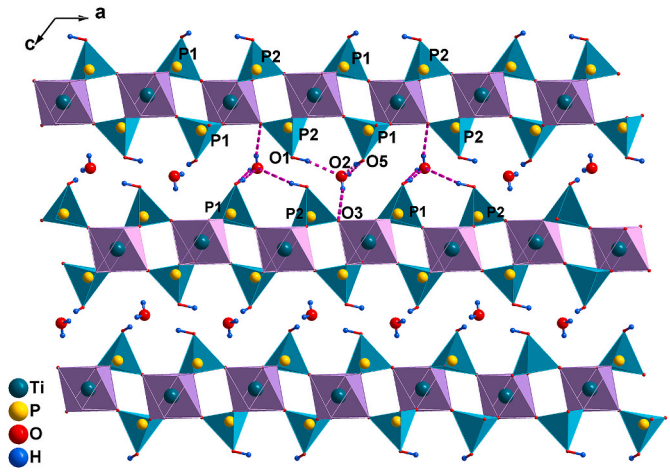

Fig. 9. Projection of the structure of α-Ti$(HPO_4)_2{\cdot}H_20$ along the *b*-axis.

through hydrogen bonds with the P–OH groups of the inorganic sheets (Table 4 and Fig. 9).

As one of the physical properties that are highly related to crystallographic structures, we chose to study the thermal behaviour of the obtained single crystals and determine whether the subtle expansion in the cell parameters led to any changes in that regard. TG-DTG-SDTA curves of α-TiP carried out in N_2-atmosphere are shown in Fig. 11 and an overlay of TG curves is shown in Fig. S4. The DTG results from the polycrystalline powder of α-TiP show three distinct minima at ≈ 60, 216 and 497 °C (Fig. 11, left panel) [63]. On the other hand, the DTG curve

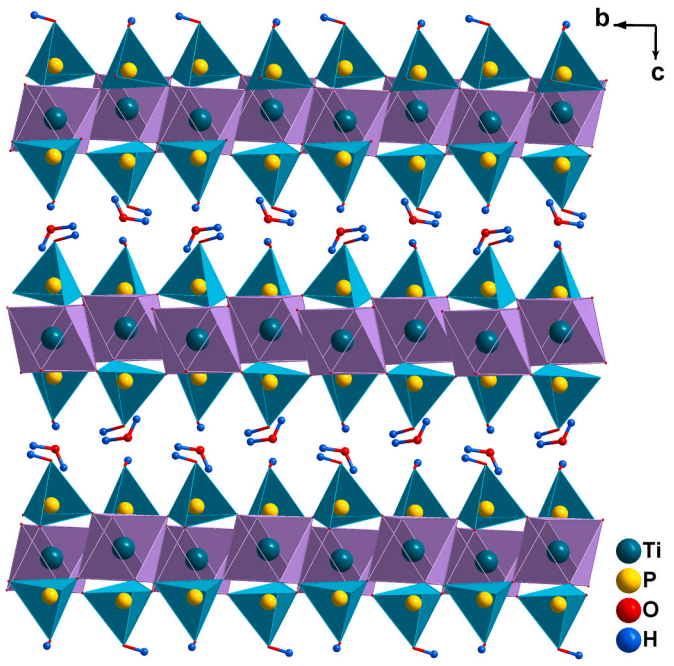

Fig. 10. Projection of the structure of α-Ti$(HPO_4)_2{\cdot}H_20$ along the a-axis.

of the single crystals shows three minima, first of which started later at 248 °C, that overlaps with another minimum at 333 °C (Fig. 11, right panel). The total mass loss of single crystals at the first and second minima is 7.2% (calculated 6.98%), corresponding to the loss of hydration water, with approximately 30% of this hydration water lost in the first band and 70% in the second one. For the single crystals, the first loss is slower (broad peak) and the second is faster (fine peak). These two minima are associated with two endothermic peaks on the SDTA at 246 °C and 336 °C. The third minimum between 450 and 800 °C is due to the elimination of condensation water with a total mass loss of 7.2% (calculated 6.98%) and minima at 553 °C (associated with an endothermic peak on the SDTA at 555 °C). This is a bit different from the DTG curve of the polycrystalline powder where the loss of hydration water at ≈ 216 °C (with the first minimum observed at 60 °C is due to the elimination of adsorbed water) and the minimum for the elimination of condensation water is reached at 497 °C, with a total mass loss of 18.3% (calculated for $Ti(HPO_4)_2{\cdot}H_2O$: 13.95%). For the same α-TiP sample, TGA was also performed under O_2-atmosphere (results not shown). The behaviour is similar (loss of hydration water: exp. 7.71%, cal. 6.98%; loss of condensation water: exp. 6.46%, cal. 6.98%). The temperature ranges are also similar to those observed in an N_2-atmosphere. So, in summary the total mass losses for single crystals is around 4% less than that of the polycrystalline powder, added to that the single crystals have started their mass loss at higher temperature than that of the polycrystalline powder, and thus it needed reaching higher temperature to complete its mass loss. This indicates that single α-TiP crystals could possess an overall higher thermal stability compared to the α-TiP polycrystalline powder.

4. Conclusions

Here, we report on a facile and novel synthesis methodology for obtaining 2D single-crystals of the α-TiP phase, suitable for single-crystal X-ray diffraction analysis. This methodology is based on the hydrothermal incubation of a titanium alloy (Ti–6Al–4V) in a concentrated phosphoric acid aqueous solution. This resulted in the controlled dissolution of titanium ion species, mostly Ti^4 (that easily forms on the titanium surface in the presence of oxygen), from the Ti–6Al–4V alloy surface and their reaction with the dissociated ions (possibly $H_2PO_4^-$, HPO_4^{2-} and/or PO_4^{3-}) of the aqueous H_3PO_4 (weak acid) under these hydrothermal conditions. Here, we suppose that due to the relatively long treatment time, the disc surface area to solution volume ratio and the used high concentration of H_3PO_4 in our experiments, the third dissociation constant of H_3PO_4 is quite small. Thus, HPO_4^{2-} was the most abundant ion that easily reacted with titanium ions (Ti^{4+}) forming the α-TiP. From our adequate observations, α-TiP is a 2D crystalline structure that undergoes apparent difficulty to proceed its growth into 3D crystals. The suggested method in this research provides means for controlled mass transport through the slow release of titanium ions into the reactive crystallization solution and this allowed for apparently low supersaturation, relatively fewer nucleation events, slower formation of the growth units (α-TiP) and, thus, better incorporation of such growth units on the growing crystal surface. On the other hand, all the results of the performed analyses (single-crystal XRD, PXRD, POM, SEM-EDX,

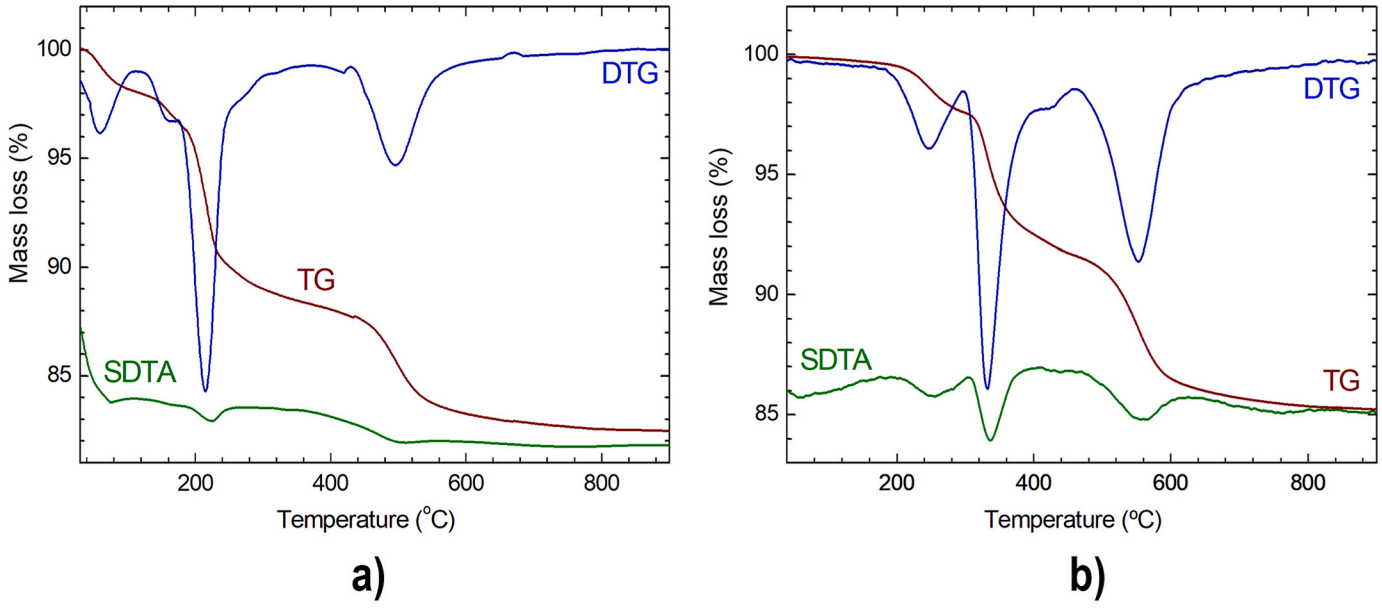

Fig. 11. TG (red line), DTG (blue line) and SDTA (green line) curves for microcrystalline powder (left panel) and single crystal (right panel) α-$Ti(HPO_4)_2{\cdot}H_20$ obtained at 10 °C/min^{-1} heating rate in N_2-atmosphere.

FTIR) agreed with what was expected and reported previously for the polycrystalline α-TiP phase. The crystallographic details obtained for α-TiP single crystals closely resemble those revealed using the polycrystalline powder of α-TiP with subtle changes in the cell parameters and distinct difference in the thermal behaviour that could indicate that α-TiP single crystals possess higher thermal stability compared to the conventional polycrystalline powder.

Funding

This work was funded by MINECO, grant numbers MAT2016-78155-C2-1-R and MCI-21-PID2020-113558RB-C41; and by the Government of the Principality of Asturias, grant number GRUPIN-IDI/2018/170. A. Adawy research is also funded through the personal grant *Ayudas Personal Técnico de Apoyo* from the Ministry of Science and Innovation, Spain (reference PTA2021-020817-I).

CRediT authorship contribution statement

Zakariae Amghouz: Conceptualization, Methodology, Software, Validation, Formal analysis, Investigation, Resources, Data curation, Writing – original draft, preparation, Visualization, Supervision, Project administration, Funding acquisition. **Rafael Mendoza-Meroño:** Methodology, Software, Validation, Formal analysis, Investigation, Resources, Data curation, All authors have read and agreed to the published version of the manuscript. **Alaa Adawy:** Conceptualization, Methodology, Validation, Formal analysis, Investigation, Resources, Data curation, Writing – original draft, preparation, Writing – review & editing, Visualization, Supervision, Project administration, Funding acquisition.

Declaration of competing interest

The authors declare that they have no known competing financial interests or personal relationships that could have appeared to influence the work reported in this paper.

Data availability

The data presented in this article is avaliable upon request from the corresponding authors. The crystallographic data is accessible at the website: https://www.ccdc.cam.ac.uk/structures/ CCDC number: 2124760.

Acknowledgments

The authors acknowledge the technical assistance of Maria Aranzazu Espina-Álvarez and Beatriz Ramajo-Escalera, from Thermal Tests and Elemental Analysis Unit, and Jorge Espina-Casado, from the electronic and vibrational spectroscopy unit, and Ángel Gutiérrez-Rodríguez, from the X-ray unit, SCTs, University of Oviedo, Spain, for the acquisition of thermal analysis data, FTIR data and preliminary X-ray data, respectively.

Appendix A. Supplementary data

Supplementary data to this article can be found online at https://doi.org/10.1016/j.jssc.2023.124251.

References

[1] K.A. Kraus, H.O. Phillips, Adsorption on inorganic materials. I. Cation exchange properties of zirconium phosphate1, J. Am. Chem. Soc. 78 (3) (1956) 694, 694.
[2] A. Clearfield, J. Stynes, The preparation of crystalline zirconium phosphate and some observations on its ion exchange behaviour, J. Inorg. Nucl. Chem. 26 (1) (1964) 117–129.
[3] G. Alberti, P. Cardini-Galli, U. Costantino, E. Torracca, Crystalline insoluble salts of polybasic metals—I Ion-exchange properties of crystalline titanium phosphate, J. Inorg. Nucl. Chem. 29 (2) (1967) 571–578.
[4] R. Llavona, M. Suarez, J.R. Garcia, J. Rodriguez, Lamellar inorganic ion exchangers. Alkali metal ion exchange on alpha-and gamma-titanium phosphate, Inorg. Chem. 28 (14) (1989) 2863–2868.
[5] U. Costantino, Intercalation of alkanols and alkylamines in insoluble acid salts of tetravalent metals having a layered structure of γ-type, J. Inorg. Nucl. Chem. 43 (8) (1981) 1895–1902.
[6] G. Alberti, U. Costantino, Recent progress in the intercalation chemistry of layered α-zirconium phosphate and its derivatives, and future perspectives for their use in catalysis, J. Mol. Catal. 27 (1–2) (1984) 235–250.
[7] A. Espina, J.B. Parra, J.R. García, J.A. Pajares, J. Rodríguez, Reactivity of alpha-titanium phosphate/n-alkylamine intercalation compounds with mono- and polymeric aluminum species, Mater. Chem. Phys. 35 (3) (1993) 250–256.
[8] P. Sylvester, R. Cahill, A. Clearfield, Pillaring of layered tetravalent metal phosphates and oxides using (3-aminopropyl) trimethoxysilane, Chem. Mater. 6 (10) (1994) 1890–1898.
[9] B. Zhang, D.M. Poojary, A. Clearfield, G. Peng, Synthesis, characterization, and amine intercalation behavior of zirconium N-(phosphonomethyl) iminodiacetic acid layered compounds, Chem. Mater. 8 (6) (1996) 1333–1340.
[10] A. Adawy, G.T. El–Bassyouni, M. Ibrahim, W.I. Abdel–Fattah, Bio nano material: the third alternative, in: N. Kumar Navani, S. Sinha (Eds.), Nanotechnology: Diagnostics and Theurapeutics, 2013. India.
[11] J. García-Glez, C. Trobajo, S.A. Khainakov, Z. Amghouz, α-Titanium phosphate intercalated with propylamine: an alternative pathway for efficient europium (III) uptake into layered tetravalent metal phosphates, Arab. J. Chem. 10 (6) (2017) 885–894.
[12] J. García-Glez, C. Trobajo, A. Adawy, Z. Amghouz, Exfoliation and europium (III)-functionalization of α-titanium phosphate via propylamine intercalation: from multilayer assemblies to single nanosheets, Adsorption 26 (2) (2020) 241–250.
[13] G.A. Albitres, S.P. Cestari, D.F. Freitas, D.C. Rodrigues, L.C. Mendes, R. Neumann, Intercalation of α-titanium phosphate with long-chain amine aided by short-chain amine, Appl. Nanosci. 10 (3) (2020) 907–916.
[14] A. Adawy, Z. Amghouz, C. Trobajo, J.R. Garcia, Antimicrobial nanolayered and nanofibrous metal phosphates for prospective biomedical applications, Acta Crystallogr. A 77 (a2) (2021) C1072.
[15] I. García, C. Trobajo, Z. Amghouz, A. Adawy, Nanolayered metal phosphates as biocompatible reservoirs for antimicrobial silver nanoparticles, Materials 14 (6) (2021) 1481.
[16] Z. Amghouz, J.R. García, A. Adawy, A review on the synthesis and current and prospective applications of zirconium and titanium phosphates, Engineering 3 (1) (2022) 161–174.
[17] A. Bortun, E. Jaimez, R. Llavona, J. García, J. Rodríguez, Formation of crystalline titanium(IV) phosphates from titanium(III) solutions, Mater. Res. Bull. 30 (4) (1995) 413–420.
[18] A.M. Krogh Andersen, P. Norby, Structural aspects of the dehydration and dehydroxylation of γ-titanium phosphate, γ-Ti(PO4)(H2PO4)·2H2O, Inorg. Chem. 37 (17) (1998) 4313–4320.
[19] L. Mafra, F.A. Almeida Paz, J. Rocha, A. Espina, S.A. Khainakov, J.R. García, C. Fernandez, Structural characterization of layered γ-titanium phosphate (C6H13NH3)[Ti(HPO4)(PO4)]·H2O, Chem. Mater. 17 (25) (2005) 6287–6294.
[20] S. Vecchio, R. Di Rocco, C. Ferragina, S. Materazzi, Thermal and kinetic study of dehydration and decomposition processes for copper intercalated γ-zirconium and γ-titanium phosphates, Themochimica Acta 435 (2) (2005) 181–187.
[21] L. Mafra, J. Rocha, C. Fernandez, G.R. Castro, S. García-Granda, A. Espina, S. A. Khainakov, J.R. García, Characterization of layered γ-titanium phosphate (C2H5NH3)[Ti(H1.5PO4)(PO4)]2·H2O intercalate: a combined NMR, synchrotron XRD, and DFT calculations study, Chem. Mater. 20 (12) (2008) 3944–3953.
[22] S. García-Granda, S.A. Khainakov, A. Espina, J.R. García, G.R. Castro, J. Rocha, L. Mafra, Revisiting the thermal decomposition of layered γ-titanium phosphate and structural elucidation of its intermediate phases, Inorg. Chem. 49 (6) (2010) 2630–2638.
[23] A.N. Christensen, E.K. Andersen, I.K. Andersen, G. Alberti, M. Nielsen11, M. Lehmann, X-ray powder diffraction study of layer compounds. The crystal structure of a-Ti (HP04) 2H20 and a proposed structure for Y-Ti(H2P04)(P04) 2H20, Acta Chem. Scand. 44 (1990) 865–872.
[24] D.M. Poojary, A.I. Bortun, L.N. Bortun, A. Clearfield, Synthesis and X-ray powder structures of three novel titanium phosphate compounds, J. Solid State Chem. 132 (1) (1997) 213–223.
[25] A. Espina, C. Trobajo, S.A. Khainakov, J.R. García, Synthesis of the fibrous materials ρ-Na0. 50H0. 50TiOPO4 and ρ-K0. 67H0. 33TiOPO4 by reaction of ρ-Ti2O(PO4)2(H2O)2 with molten alkali nitrates, Mater. Res. Bull. 36 (13–14) (2001) 2531–2541.
[26] A. Espina, C. Trobajo, S.A. Khainakov, J.R. García, M.A. Salvadó, P. Pertierra, S. García-Granda, Reaction of π-Ti2O(PO4)2· 2H2O with molten alkali nitrates: synthesis of the fibrous materials π-M0. 5H0. 5TiOPO4 (M= Na, K), Mater. Res. Bull. 37 (8) (2002) 1381–1392.
[27] V.A. Burnell, J.E. Readman, C.C. Tang, J.E. Parker, S.P. Thompson, J.A. Hriljac, Synthesis and structural characterisation using Rietveld and pair distribution function analysis of layered mixed titanium–zirconium phosphates, J. Solid State Chem. 183 (9) (2010) 2196–2204.
[28] A.A. Babaryk, A. Adawy, I. García, C. Trobajo, Z. Amghouz, R.M. Colodrero, A. Cabeza, P. Olivera-Pastor, M. Bazaga-García, L. dos Santos-Gómez, Structural and proton conductivity studies of fibrous π-Ti2O(PO4)2· 2H2O: application in chitosan-based composite membranes, Dalton Trans. 50 (22) (2021) 7667–7677.

[29] V. Bakhmutov, A. Contreras, H. Drake, H.-C. Zhou, Elucidating structure and dynamics of crystalline α-zirconium phosphates intercalated with water and methanol by multinuclear solid-state MAS NMR: a comprehensive NMR approach, Magn. Reson. Chem. 60 (6) (2022) 541–553.
[30] A. Chernov, Modern Crystallography III: Crystal Growth, Springer-Verlag, Munich, Germany, 1984.
[31] R. Lacmann, A. Herden, C. Mayer, Kinetics of nucleation and crystal growth, Chem. Eng. Technol. 22 (4) (1999) 279–289.
[32] A.S. Myerson, R. Ginde, Crystals, crystal growth, and nucleation, in: A.S. Myerson (Ed.), Handbook of Industrial Crystallization, Elsevier, 2002, pp. 33–65.
[33] J. McGinty, N. Yazdanpanah, C. Price, J.H. Ter Horst, J. Sefcik, Nucleation and crystal growth in continuous crystallization, in: N. Yazdanpanah, Z.K. Nagy (Eds.), The Handbook of Continuous Crystallization, RSC, 2020, pp. 1–50.
[34] A. Ducruix, R. Giegé, Crystallization of Nucleic Acids and Proteins: a Practical Approach, Oxford University Press, Oxford, New York, USA, 1999.
[35] H.-H. Tung, E.L. Paul, M. Midler, J.A. McCauley, Crystallization of Organic Compounds: an Industrial Perspective, John Wiley & Sons, 2009.
[36] A. Adawy, K. Marks, W.J. De Grip, W.J.P. van Enckevort, E. Vlieg, The development of the depletion zone during ceiling crystallization: phase shifting interferometry and simulation results, CrystEngComm 15 (12) (2013) 2275–2286.
[37] A. Adawy, W. Corbeek, E. de Ronde, W.J. van Enckevort, J. Willem, E. Vlieg, A practical kit for micro-scale application of the ceiling crystallisation method, CrystEngComm 17 (13) (2015) 2602–2605.
[38] A. Adawy, Z. Amghouz, J.C.M. van Hest, D.A. Wilson, Sub-micron polymeric stomatocytes as promising templates for confined Crystallization and Diffraction Experiments, Small 13 (28) (2017), 1700642.
[39] A. Contreras, S. Tao, G. Day, V. Bakhmutov, S. Billinge, H.-C. Zhou, Zirconium phosphate: the pathway from turbostratic disorder to crystallinity, Inorg. Chem. 58 (20) (2019) 14260–14274.
[40] G. Alberti, U. Costantino, S. Allulli, M. Massucci, M. Pelliccioni, Crystalline insoluble acid salts of tetravalent metals—XV the influence of preparation methods on the ion-exchange behaviour of crystalline zirconium phosphate, J. Inorg. Nucl. Chem. 35 (4) (1973) 1347–1357.
[41] A. Nilchi, M. Ghanadi Maragheh, A. Khanchi, M. Farajzadeh, A. Aghaei, Synthesis and ion-exchange properties of crystalline titanium and zirconium phosphates, J. Radioanal. Nucl. Chem. 261 (2) (2004) 393–400.
[42] A. Adawy, W. I Abd El-Fattah, E.-S. M El-Sayed, M.S. Talaat, Biomimetic coating of precalcified Ti-6Al-4V alloy, Open Med. Dev. J. 1 (1) (2009) 19–28.
[43] I. García, C. Trobajo, Z. Amghouz, M. Alonso-Guervos, R. Díaz, R. Mendoza, M. Mauvezín-Quevedo, A. Adawy, Ag-and Sr-enriched nanofibrous titanium phosphate phases as potential antimicrobial cement and coating for a biomedical alloy, Mater. Sci. Eng. C 126 (2021), 112168.
[44] M.A. Salvado, P. Pertierra, S. Garcia-Granda, J.R. Garcia, J. Rodriguez, M. T. Fernandez-Diaz, Neutron powder diffraction study of [alpha]-Ti(HPO4)2.H2O and [alpha]-Hf(HPO4)2.H2O; H-atom positions, Acta Crystallogr. B 52 (5) (1996) 896–898.
[45] Z. Amghouz, R. Mendoza-Merono, S. Garcia-Granda, A. Adawy, Nucleation and growth of [alpha]-Ti(HPO4)2.H2O single crystal and its unprecedented structure determination from X-ray single-crystal data, Acta Crystallogr. A 78 (a2) (2022) e734.
[46] M.C. Burla, R. Caliandro, B. Carrozzini, G.L. Cascarano, C. Cuocci, C. Giacovazzo, M. Mallamo, A. Mazzone, G. Polidori, Crystal structure determination and refinement via SIR2014, J. Appl. Crystallogr. 48 (1) (2015) 306–309.
[47] L.J. Bourhis, O.V. Dolomanov, R.J. Gildea, J.A.K. Howard, H. Puschmann, The anatomy of a comprehensive constrained, restrained refinement program for the modern computing environment - Olex2 dissected, Acta Crystallogr. A 71 (1) (2015) 59–75.
[48] J.R. Carvajal, Recent developments of the program FULLPROF, in commission on powder diffraction (IUCr), Newsletter 26 (2001) 12–19.
[49] V. Singh, S. Hosseini, Corrosion behaviour of Ti-6Al-4V in phosphoric acid, J. Appl. Electrochem. 24 (3) (1994) 250–255.
[50] J.-s. Lu, Corrosion of titanium in phosphoric acid at 250 C, Trans. Nonferrous Metals Soc. China 19 (3) (2009) 552–556.
[51] M. Khadiri, M. Elyaagoubi, R. Idouhli, Y. Koumya, O. Zakir, J. Benzakour, A. Benyaich, A. Abouelfida, A. Outzourhit, Electrochemical study of anodized titanium in phosphoric acid, Adv. Mater. Sci. Eng. 2020 (2020).
[52] H. Ortiz-Oliveros, R.M. Flores-Espinoza, E. Ordonez-Regil, S. Fernández-Valverde, Synthesis of a-Ti(HPO4)2.H2O and sorption of Eu(III), Chem. Eng. J. 236 (2014) 398–405.
[53] Q. Wang, L. Zhong, J. Sun, J. Shen, A facile layer-by-layer adsorption and reaction method to the preparation of titanium phosphate ultrathin films, Chem. Mater. 17 (13) (2005) 3563–3569.
[54] P.L. Stanghellini, E. Boccaleri, E. Diana, G. Alberti, R. Vivani, Vibrational study of some layered structures based on titanium and zirconium phosphates, Inorg. Chem. 43 (18) (2004) 5698–5703.
[55] Z. Barhon, A. Albizane, M. Azzi, N. Saffaj, J. Bennazha, S.Y. Unssi, Effect of silver activation of zirconium phosphate on the methylene blue adsorption, J. Appl. Sci. Res. 5 (2009) 893–904.
[56] M. Maslova, L. Gerasimova, The influence of chemical modification on structure and sorption properties of titanium phosphates, Russ. J. Appl. Chem. 84 (2011) 1–8.
[57] H. Qiao, F. Jia, Z. Ai, Z. Li, L. Zhang, One-pot synthesis of spring-like superstructures consisting of layered tin (IV) hydrogen phosphate nanodisks, Chem. Commun. (19) (2006) 2033–2035.
[58] A. Adawy, W.J.P. van Enckevort, E.S. Pierson, W.J. de Grip, E. Vlieg, Illuminating protein crystal growth using fluorophore-labelled proteins, CrystEngComm 16 (42) (2014) 9800–9809.
[59] A. Adawy, E.G. van der Heijden, J. Hekelaar, W.J. van Enckevort, W.J. de Grip, E. Vlieg, A comparative study of impurity effects on protein crystallization: diffusive versus convective crystal growth, Cryst. Growth Des. 15 (3) (2015) 1150–1159.
[60] R.B. Ravelli, S.M. McSweeney, The 'fingerprint'that X-rays can leave on structures, Structure 8 (3) (2000) 315–328.
[61] T. Degen, M. Sadki, E. Bron, U. König, G. Nénert, The highscore suite, Powder Diffr. 29 (S2) (2014) S13–S18.
[62] C. Groom, I. Bruno, M. Lightfoot, S. Ward, The cambridge structural database, Acta Crystallogr. B: Struct.Sci. Crystal Eng. Mater. 72 (2) (2016) 171–179.
[63] J. García-Glez, O. Khainakova, I. Iglesias, B.F. Alfonso, J.A. Huidobro, Z. Amghouz, A. Espina, C. Trobajo, Thermal behavior of layered α-titanium phosphates: from the titanium (IV) bis (hydrogenphosphate) monohydrate to an europium (III)-phase via propylamine intercalation, J. Therm. Anal. Calorim. 134 (1) (2018) 797–805.